Chinese Journal of Chemical Engineering 85 (2025) 251–259

Contents lists available at ScienceDirect

Chinese Journal of Chemical Engineering

journal homepage: www.elsevier.com/locate/CJChE

Full Length Article

Stability investigation and techno-economic assessment of gliding arc plasma coupled electrocatalytic ammonia synthesis system

Yang Lv, Gaoyang Li, Jianpeng Sun, Honghui Ou, Yang Li *, Guidong Yang *

State Key Laboratory of Fluorine & Nitrogen Chemicals, School of Chemical Engineering and Technology, Xi'an Jiaotong University, Xi'an 710049, China

ARTICLE INFO

Article history:
Received 23 March 2025
Received in revised form
21 April 2025
Accepted 22 April 2025
Available online 17 May 2025

Keywords:
Ammonia synthesis
Plasma
Electrochemistry
Equilibrium
Response surface analysis
Economics

ABSTRACT

The plasma-coupled electrocatalytic cascade technology with NO_x^- as intermediate product is a potential method to realize green ammonia synthesis. The matching of the formation rate and consumption rate of NO_2^- as the main absorption product is an important prerequisite for the system to achieve stable operation. Therefore, this paper firstly emphasizes the importance of operating parameters on the cascade system based on the single factor experiment. Secondly, the empirical equation between electrocatalytic operating conditions and NO_2^- consumption rate was established by response surface analysis. Based on this equation, the electrocatalytic operating parameters were optimized to achieve the dynamic equilibrium between NO_2^- formation rate and consumption rate. Finally, the techno-economic assessment model was established to calculate the levelized cost of ammonia based on the cascade system, and the single-variable sensitivity analysis was performed to provide the clear guidance for cost reduction.

1. Introduction

Ammonia, as the iconic commodity goods that launched the modern chemical industry, has important applications in agriculture, chemical industry, electronic industry and food industry [1–3]. Meanwhile, ammonia has also attracted much attention in the energy field as a clean and efficient hydrogen energy carrier [4–6]. As the main technology for industrial ammonia synthesis, the Haber-Bosch method has produced 90% of the world's artificial ammonia products [7], solving the food problem for more than 40% of the world's population [8]. However, this technology has harsh reaction conditions (400–600 °C, 20–40 MPa), high carbon emissions, and relies on complex large-scale equipment and production processes [9–11], which gradually contradicts with the context of advocating energy conservation and emission reduction, and promoting the balanced allocation of global resources. Therefore, it is urgent to explore new technologies for large-scale industrialized green ammonia synthesis with low energy consumption and carbon emission [12–15]. In recent years, the plasma-coupled electrocatalytic ammonia synthesis cascade process using air and water as feedstock, driven by green electricity, and under ambient temperature and pressure has become a potential method for miniaturization, decentralization, and localization of industrial green ammonia synthesis due to its simple equipment as well as cheap and readily available feedstock [16–18].

The plasma-coupled electrocatalytic ammonia synthesis process is shown in Fig. 1. The cascade system is mainly composed of three modules: N_2 activation, chemical absorption of NO_x, and electrochemical reduction of NO_x^- [19]. First, the compressed air is fed into the plasma generator and the excited high-energy electrons collide inelastically with inert gas molecules to produce highly reactive species, such as vibrationally active nitrogen $N_2(v)$, vibrationally active oxygen $O_2(v)$, nitrogen atoms (N) and oxygen atoms (O), and these reactive species will further react to generate NO and NO_2, as shown in the Reactions (1)–(3). Subsequently, the NO_x containing plasma outlet gas is absorbed by alkaline electrolyte in the absorption module, as shown in Reactions (4) and (5) [20]. It should be noted that the concentration of NO_2^- in the liquid phase product is far higher than that of NO_3^- [21,22]. Finally, the electrolyte containing NO_2^- is reduced to NH_3 in the cathodic chamber of the electrochemical reactor, while oxygen evolution reaction occurs at the anode as shown in Reactions (6) and (7), respectively [23,24].

* Corresponding authors.
E-mail addresses: yangli0528@xjtu.edu.cn (Y. Li), guidongyang@xjtu.edu.cn (G. Yang).

https://doi.org/10.1016/j.cjche.2025.04.014

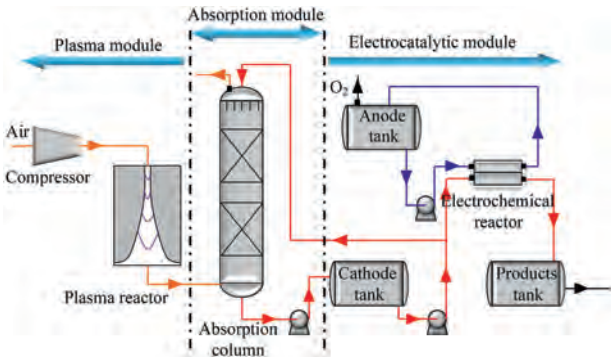

Fig. 1. Technological process diagram of plasma-coupled electrocatalysis system for ammonia synthesis.

$$N_2(v) + O \rightarrow NO + N \quad (1)$$

$$O_2(v) + N \rightarrow NO + O \quad (2)$$

$$NO_2NO + O \rightarrow 2NO_2 \quad (3)$$

$$2NO_2 + 2OH^- \rightarrow NO_2^- + NO_3^- + H_2O \quad (4)$$

$$NO_2 + NO + 2OH^- \rightarrow 2NO_2^- + H_2O \quad (5)$$

$$4OH^- \rightarrow O_2 + 2H_2O + 4e^- \quad (6)$$

$$NO_2^- + 5H_2O + 6e^- \rightarrow NH_3 + 7OH^- \quad (7)$$

The long-term stable operation of plasma-coupled electrocatalytic ammonia synthesis cascade system is of irreplaceable significance for the guarantee of the main technical indexes such as ammonia production efficiency, product quality and technical economy. Among them, NO_2^- as the main product of plasma outlet gas after chemical absorption, the matching of its formation rate and consumption rate is the key to realize the long-term stable operation of the system, and is also the basis for guaranteeing the continuity and high selectivity of the whole ammonia production process. However, the current research on the cascade system only focuses on the in-depth development of cathode catalytic materials, neglecting the investigation of the internal dynamic balance of the system as well as the in-depth understanding of the mechanism of influencing the operating conditions of the system and the strict control of the process parameters. Therefore, the gliding arc plasma-coupled electrocatalytic experimental platform was designed and constructed in this paper, and the effects of the core operating parameters on the ammonia formation rate were systematically investigated. Besides, the empirical equation for predicting the ammonia formation rate under different combinations of electrocatalytic operating parameters was developed by using response surface analysis method, which enabled precise regulation of the NO_2^- consumption rate and ultimately the stable operation of the cascade system. Finally, a techno-economic assessment model of gliding arc plasma-coupled electrocatalytic cascade system is developed aiming to provide guidance for the deeply optimization of the cascade system from an economic perspective. The results of this paper contribute to an in-depth understanding of the influence mechanism of multiple operating conditions on the key processes in cascade system, and provide technical support and solutions to ensure the stable operation of the system and reduce the levelized cost of ammonia.

2. Experimental Equipment and Method

The experimental platform, shown in Fig. 2, consists of the carrier gas system, high-frequency and high-voltage discharge system, gliding arc plasma (GAP) reactor, electrocatalytic DC regulated power supply, electrochemical reactor, electrolyte circulation system and exhaust gas absorption system. The plasma reactor shell is made of quartz for convenient observation of the arc ignition and gliding behavior at the electrode gap, and the arc-inducing dual electrodes are made of 3D printed stainless steel. The main structure of the electrochemical flow cell reactor is shown in Fig. S1, which consists of the titanium current collector with serpentine flow channels, a cathode catalyst (copper foam with the geometric area of 100 cm^2), a proton exchange membrane (Nafion 117), and an anode catalyst (nickel foam with the geometric area of 100 cm^2).

It should be noted that the air flow rate, plasma generator input voltage, electrocatalytic cell voltage and cathode electrolyte flow rate were adjusted according to different experimental purposes, while the electrolyte flow rate of the anode-side was fixed at 50 $ml \cdot min^{-1}$, and the cathode and anode electrolytes were both 1 $mol \cdot L^{-1}$ KOH solutions. Prior to any experiments, it is necessary to ensure that the whole system was well sealed to avoid any possible leakage. In addition, the copper foam was reduced in 1 $mol \cdot L^{-1}$ KOH for 2.5 h at 25 A to activate the electrode. NH_3 and NO_2^- were quantified by UV spectrophotometry [25,26], as detailed in the Supporting Information.

3. Results and Discussion

3.1. Single factor experiment

3.1.1. Plasma generator input voltage

The effects of plasma generator input voltage on the NO_2^- formation rate ($R_{NO_2^-}$), NO_2^- initial concentration (C_{0,NO_2^-}) and NH_3 formation rate (R_{NH_3}) were investigated under the conditions of 4 $L \cdot min^{-1}$ air flow rate, 2.00 V electrocatalytic cell voltage, and 60 $ml \cdot min^{-1}$ cathode electrolyte flow rate, the experimental results are shown in Fig. 3. Fig. 3(a)–(b) illustrate that the $R_{NO_2^-}$ and C_{0,NO_2^-} exhibit a nearly linear relationship with the increasing plasma generator input voltage, which was attributed to the fact that the N_2 and O_2 could obtain more energy through inelastic collisions with high-energy electrons, so as to promote the generation of multiple

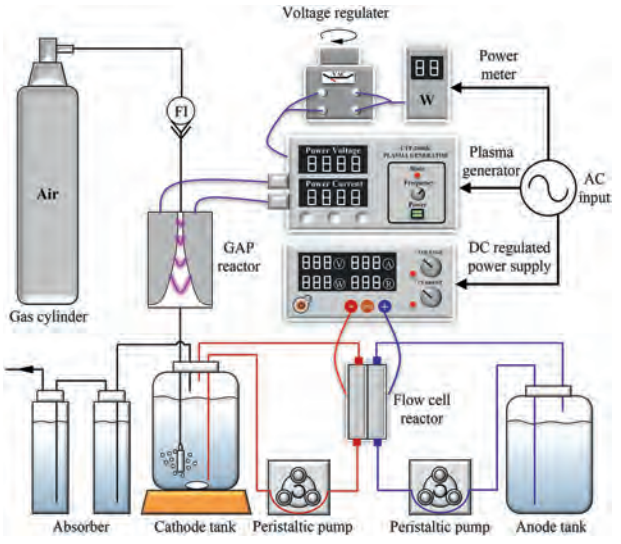

Fig. 2. Schematic diagram of experimental system.

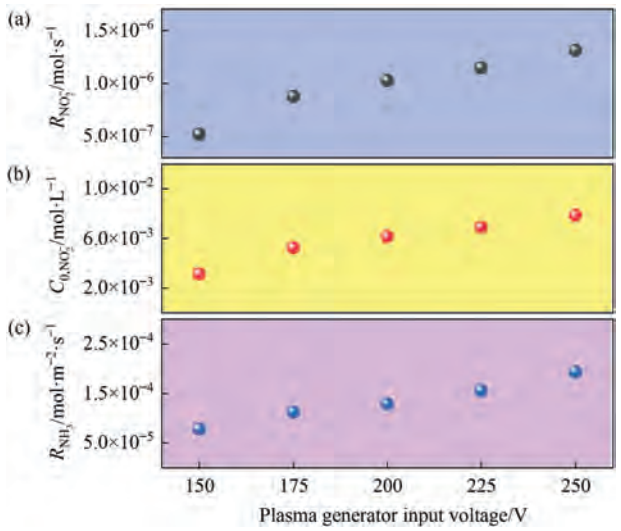

Fig. 3. The effects of plasma generator input voltage on (a) $R_{NO_2^-}$, (b) C_{0,NO_2^-} and (c) R_{NH_3}

reactive species dominated by $N_2(v)$, $O_2(v)$, N and O [27], and thus more NO_2^- were produced by chemical absorption. In the electrocatalytic process, the high initial reactant concentration will increase the concentration gradient at the interface between the cathode and electrolyte, which enhances the concentration diffusion process [28]. The strengthened mass transfer process then contributes to the promotion of the electrochemical NO_2^- reduction reaction, so the R_{NH_3} shows the similar variation trend as the C_{0,NO_2^-}, as depicted in Fig. 3(c).

In addition, the variation curves of NO_2^- concentration ($C_{NO_2^-}$) and NH_3 concentration (C_{NH_3}) during a complete experimental period at the plasma generator input voltage of 200 V were monitored, the results are shown in Fig. 4. The $C_{NO_2^-}$ increased steadily and linearly during the plasma-only operation duration, and the C_{NH_3} also showed the linear variation during the cascade system operation duration, indicating that the experimental system has reliably stable. However, it is obvious that the $C_{NO_2^-}$ within the experimental system continues decreasing at electrocatalytic initiation, which is attributed to the mis-match between the NO_2^- formation rate of the GAP and the NO_2^- consumption rate of the electrocatalysis. It can be anticipated that this disequilibrium phenomenon will result in the experimental system being incapable of sustaining its current stability over extended experimental duration.

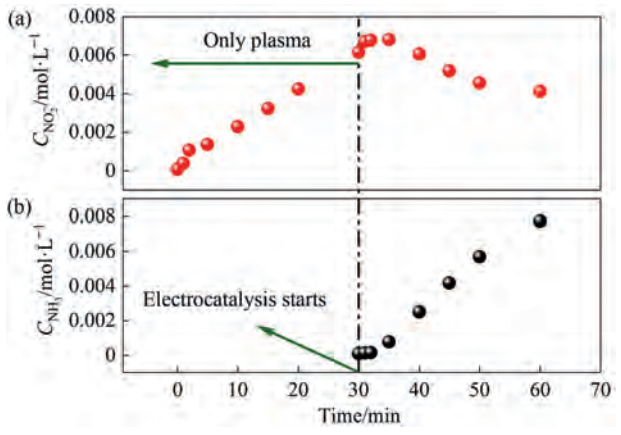

Fig. 4. Evolutions of (a) $C_{NO_2^-}$ and (b) C_{NH_3} over reaction time.

3.1.2. Gas flow rate

For the GAP module, the influence of inlet gas flow rate on the cascade system is illustrated in Fig. 5. The potential impacts of increasing flow rate on the $R_{NO_2^-}$ are mainly reflected in two-fold. On the one hand, high gas velocity is beneficial to prolong the arc gliding distance, enhances the fluid turbulence degree, and exacerbate the non-equilibrium degree, which collectively improves the probability of inelastic collisions between N_2, O_2, and energetic electrons for improving N_2 activation and NO_x formation [29]; On the other hand, high gas velocity shortens the gas residence time in absorption liquor, which is disadvantageous to the chemical absorption at the gas-liquid interface. In summary, the synergistic interplay between the positive effects of increased gas velocity on N_2 activation and its negative impacts on chemical absorption results in the nonlinear variation in $R_{NO_2^-}$ with increasing gas flow rate. Similar to Fig. 3(c), the concentration effects of electrocatalytic reactant results in the same variation trend of R_{NH_3} as that of C_{0,NO_2^-}, which indicates that the mass transfer process of NO_2^- is the critical factor affecting the R_{NH_3} at the cell voltage of 2.00 V.

3.1.3. Cell voltage

The effects of electrocatalytic cell voltage on the cascade system were examined, and the experimental results are shown in Fig. 6. Fig. 6(a) demonstrates the accumulated NO_2^- content in electrolyte after 30 min of GAP-activated N_2 in five parallel experiments, which shows the acceptable data repeatability with the maximum positive deviation of +3.68%, the maximum negative deviation of −7.69%, and the average deviation of 3.08%. Additionally, approximately same C_{0,NO_2^-} also contributes to eliminating the influence of concentration effects as mentioned previously on the results of electrocatalytic module.

For a typical interfacial electrochemical reaction process, the apparent reaction rate is mainly restricted by two aspects: the electrochemical kinetics restriction and species mass transfer restriction [30]. The nonlinear variation of R_{NH_3} with increasing electrolytic cell voltage as shown in Fig. 6(b) demonstrates the transition from kinetics restriction to mass transfer restriction in the process of electrocatalytic NO_2^- reduction reaction for NH_3 synthesis. Concretely, when the interfacial reaction is under the kinetics restriction implies that the reaction rate is less than the mass transfer rate, thus increasing the cell voltage will significantly improves the activation overpotential which is employed to characterize the driving force of electrochemical reaction, and taps into

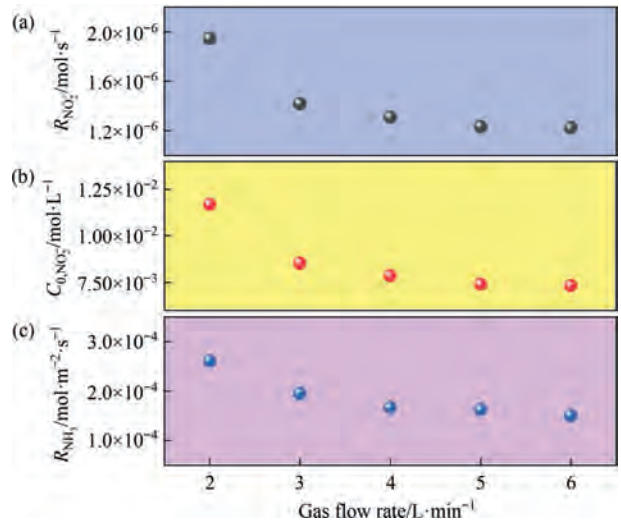

Fig. 5. The effects of plasma inlet gas flow rate on (a) $R_{NO_2^-}$, (b) C_{0,NO_2^-} and (c) R_{NH_3}

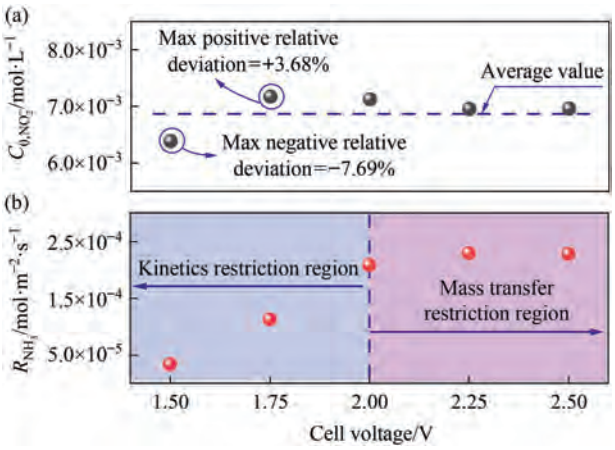

Fig. 6. (a) C_{0,NO_2^-} and (b) R_{NH_3} under different cell voltages.

a visibly higher R_{NH_3}, such as the cell voltage is increased from 1.50 V to 2.00 V. Notably, as interfacial reaction is restricted by the species mass transfer, *i.e.*, the reaction rate is larger than the species mass transfer rate, at that point the mass transfer process of the reactants from the bulk fluid to the solid-liquid interface becomes the critical determinant of the R_{NH_3}. Consequently, sustained increases in electrocatalytic cell voltage will not continue to enhance the R_{NH_3}, *e.g.*, the cell voltage increases from 2.00 V to 2.50 V. It can be expected that the excessive increasing cell voltage did not have any positive impacts on R_{NH_3}, which resulted in lower energy efficiency.

3.1.4. Cathode electrolyte flow rate

In this section, the effects of cathode electrolyte flow rate on R_{NH_3} are discussed. The species mass transfer process in electrocatalytic system can be mainly categorized into three types: forced convection driven by external force, concentration diffusion driven by concentration gradient and ionic electromigration driven by potential gradient [31,32], as shown in Fig. 7(a). The R_{NH_3} at different electrolyte flow rates are shown in Fig. 7(b). The elevated electrolyte flow rate promotes electrochemical reactions through both direct and indirect mechanisms. Directly, increasing electrolyte flow rate contributes to enhancing the turbulence degree of the bulk fluid, which strengthens the internal mixing, and synchronously boosts the velocity component in the direction perpendicular to the electrode, which further facilitates the species renewal at the solid-liquid interface. Indirectly, the increased flow rate promotes the concentration-diffusion process by raising the wall shear stress which reduces the thickness of concentration boundary layer resulting in an improved concentration gradient [28]. In summary, the mechanism of increased R_{NH_3} caused by cathode electrolyte flow rate is essentially the facilitation of interfacial electrochemical reaction by the enhanced species mass transfer process in the reactor.

3.2. Stability optimization of the cascaded system

As previously mentioned, the matching between the formation rate and consumption rate of NO_2^-, which serves as the nexus between the gliding arc plasma module and the electrocatalytic module, is crucial to achieve stable operation of the cascade system. Consequently, in this section, response surface analysis (RSA) was employed to establish an empirical equation correlating the NO_2 consumption rate during the electrocatalytic NO_2 reduction process with cell voltage, electrolyte flow rate, and NO_2 concentration. With the objective of equalizing the NO_2^- formation rate ($R_{NO_2^-}$) of the gliding arc plasma with the NO_2^- consumption rate ($-R_{NO_2^-}$) of the electrocatalytic process, the RSA-derived empirical equation was utilized to identify the combination of electrocatalytic operation parameters that align with $R_{NO_2^-}$. This approach ultimately facilitated the dynamic equilibrium between NO_2^- formation rate and NO_2^- consumption rate during a continuous 10-h operation of the cascade system.

3.2.1. Response surface analysis of electrocatalytic NO_2^- reduction to NH_3

The repeatability of experimental data is the essential basis for ensuring the empirical equation has accurate. Therefore, the electrocatalysis module was verified for experimental repeatability at the same operating conditions (2.00 V, 60 ml·min^{-1} and 0.03 mol·L^{-1}), and the results are shown in Fig. 8. The maximum deviation of five parallel experiments is 6.58%, and the average relative

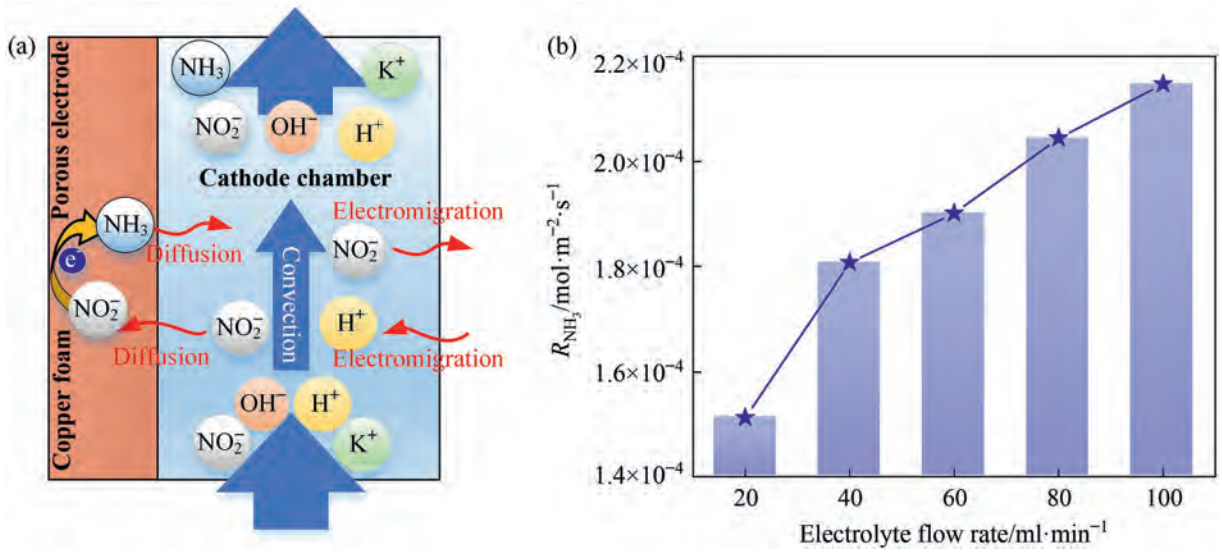

Fig. 7. (a) Schematic diagram of species mass transfer in the electrocatalytic system, and (b) effects of electrolyte flow rate on R_{NH_3}.

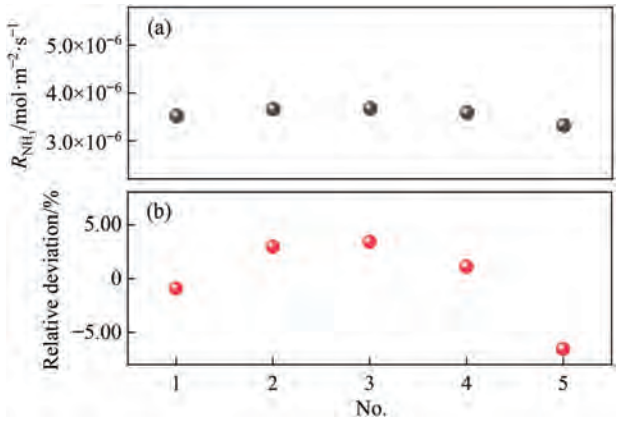

Fig. 8. (a) R_{NH_3} and (b) relative deviation of five parallel electrocatalytic experiments.

deviation is 3.00%, which shows acceptable experimental repeatability.

Moreover, the response surface analysis method was used to establish the NO_2^- consumption rate equation related to the operating parameters within the electrocatalytic module, in order to achieve the preferred combination of electrocatalytic operating parameters, so as to realize the dynamic equilibrium of $C_{NO_2^-}$ in the electrolyte, *i.e.*, the NO_2^- formation rate is equal to the NO_2^- consumption rate. Specifically, the Design Expert V10.0 software was firstly utilized to design the experimental protocols by using the central composite design method. Among them, the cell voltage, NO_2^- initial concentration and cathode electrolyte flow rate are critical factors, and the R_{NH_3} is response value. It should be emphasized that the NO_2^- initial concentration in the cascade system is the variable which is related to the plasma operation conditions and accumulation time, whereas the NO_2^- initial concentration in this part is obtained from the KNO_2 solution in gradient configuration. The designed experimental protocols are shown in Table 1.

The results corresponding to the above experimental protocols are presented in Fig. 9. It should be particularly emphasized that the NO_2^- concentration of the artificially-configured solution within this experimental system will decline significantly with experimental duration. To minimize the excessive consumption of NO_2^-, each experiment in this section was set to 5 min. Excessive consumption of feedstock would lead to the concentration effects as described previously, which leads to undesired low R_{NH_3}, and thus affects the subsequent match between $R_{NO_2^-}$ and $-R_{NO_2^-}$, and this R_{NH_3} which is influenced by the reduction in reactant concentration is defined as the time-averaged ammonia formation rate. In contrast, the R_{NH_3} that excludes the effects of reactant concentration on the electrocatalytic module is referred to as the instantaneous ammonia formation rate. Fig. 9(b) shows that the NO_2^- conversion rate remained low under all experimental conditions, and it can be regarded as the experimental system being essentially independent of concentration effects, thus beneficially guaranteeing the relatively small difference between the time-averaged ammonia formation rate and instantaneous ammonia formation rate.

Table 1
Experimental protocols.

NO.	Cell voltage/V	Flow rate/ml·min^{-1}	NO_2^- concentration/mol·L^{-1}
1	1.50	60	0.03
2	1.75	40	0.04
3	1.75	80	0.02
4	1.75	80	0.04
5	1.75	40	0.02
6	2.00	60	0.03
7	2.00	100	0.03
8	2.00	60	0.05
9	2.00	20	0.03
10	2.00	60	0.01
11	2.25	80	0.02
12	2.25	40	0.02
13	2.25	40	0.04
14	2.25	80	0.04
15	2.50	60	0.03

Subsequently, the empirical equation between the factors and response value was established by fitting the experimental results with multiple regressions, as shown Eq. (8):

$$R_{NH_3} = -R_{NO_2^-} - 1.567 \times 10^{-7} - 2.49452 \times 10^{-6} \cdot A \quad (8)$$

$$-3.590 \times 10^{-8} \cdot B - 9.009 \times 10^{-6} \cdot C + 1.184 \times 10^{-8} \cdot A \cdot B$$

$$+2.415 \times 10^{-5} \cdot A \cdot C - 2.369 \times 10^{-7} \cdot B \cdot C$$

$$+1.942 \times 10^{-6} \cdot A^2 + 1.885 \times 10^{-10} \cdot B^2$$

$$+8.615 \times 10^{-5} \cdot C^2$$

where A represents the cell voltage, B is the electrolyte flow rate, and C represents the initial concentration of NO_2^-.

Table 2 shows the analysis of variance (ANOVA) of the previous empirical equation. The F-value of the model is 241.61 with P-value <0.0001, indicating that the equation is highly significant and reliable. Further, the P-value of cell voltage <0.0001 indicates that this term has the highly significant effects on the R_{NH_3}. When 0.0001 < P-value <0.05, it indicates that the terms have the significant effects on R_{NH_3}, such as the NO_2^- initial concentration and the square of cell voltage. The P-value >0.05 for the rest of the terms indicates that these parameters are not significant for R_{NH_3}. In addition, the multiple correlation coefficient R^2 = 0.9977 in the ANOVA indicates that this empirical equation fits well; the adj R^2 = 0.9936 and the pred R^2 = 0.9782 are close to each other, which indicates that this empirical equation can reflect the relationship between experimental values and predicted values well, *i.e.*, this equation has the high reliability and prediction accuracy; the adeq precision = 55.95 > 4, indicating that this equation has enough precision to describe the data variation.

Finally, the experiments involved in Table 1 were re-predicted based on the empirical equation and the results are shown in Fig. 10. The results show that the maximum and average prediction error is −8.46% and 2.30% respectively, which shows an acceptable prediction precision, thus confirming the accuracy of the above equation.

3.2.2. Cascade system stability verification

In order to verify the correctness of the empirical equation, a 10 h experiment was carried out. Here, the plasma generator input voltage was fixed at 200 V and the air flow rate was fixed at 4.0 L·min^{-1}, while the electrocatalytic operating parameters were obtained from Design Expert V10.0 based on the previous empirical equation, specifically, the cell voltage was 1.635 V, the cathode electrolyte flow rate was 65.254 ml·min^{-1} and the initial concentration of NO_2 was 0.023 mol·L^{-1}. Considering the precision of experimental equipment and the feasibility of experimental protocol, the actual cell voltage, electrolyte flow rate and initial concentration of NO_2^- were set to 1.64 V, 65 ml·min^{-1} and 0.023

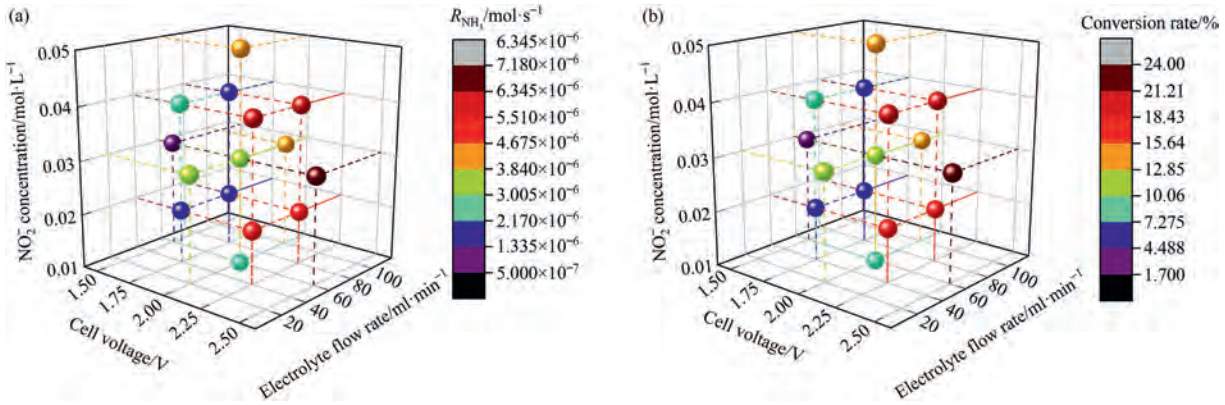

Fig. 9. Results of electrocatalytic RSA experiments. (a) R_{NH_3}, and (b) conversion rate.

Table 2
ANOVA results.

Source	Sum of squares	df	Mean square	*F*-value	*P*-value
Model	4.686×10^{-11}	9	5.207×10^{-12}	241.61	<0.0001
A	4.498×10^{-11}	1	4.498×10^{-11}	2087.14	<0.0001
B	6.996×10^{-14}	1	6.996×10^{-14}	3.25	0.1315
C	1.463×10^{-12}	1	1.463×10^{-12}	67.91	0.0004
AB	2.806×10^{-14}	1	2.806×10^{-14}	1.30	0.3055
AC	2.916×10^{-14}	1	2.916×10^{-14}	1.35	0.2927
BC	1.796×10^{-14}	1	1.796×10^{-14}	0.83	0.4032
A^2	1.631×10^{-13}	1	1.631×10^{-13}	7.57	0.0403
B^2	6.299×10^{-14}	1	6.299×10^{-14}	2.92	0.1480
C^2	8.222×10^{-16}	1	8.222×10^{-16}	0.038	0.8528
Residual	1.078×10^{-13}	5	2.155×10^{-14}		
Cor total	4.697×10^{-11}	14			

Note: $R^2 = 0.9977$; adj $R^2 = 0.9936$; pred $R^2 = 0.9782$; adeq precision = 55.95.

mol·L^{-1}, respectively. It needs to be explained that the initial concentration of NO_2^- in this experiment was provided by an individual running of the GAP module. After the experiment, the system stability was illustrated by detecting the fluctuation of NO_2^- concentration, and the results are shown in Fig. 11.

The linear accumulation of NO_2^- in the GAP module over the experimental duration is critical to ensure that the initial concentration is consistent with the experimental protocol. Based on the average yields in Fig. 6(a), the NO_2^- accumulation concentration of 0.0233 mol·L^{-1} consistent with the expectation was obtained by

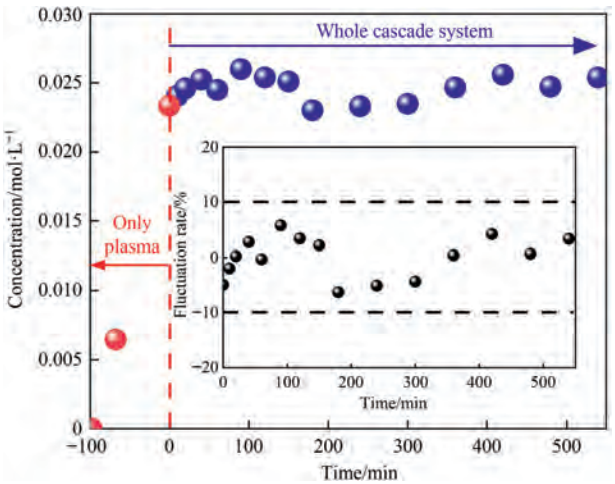

Fig. 11. The variation curve and fluctuation rate of NO_2^- concentration.

operating the GAP module alone for 98 min. During the operation period of the gliding arc plasma-coupled electrocatalytic system, the concentration of NO_2^-, which is the link between GAP and electrocatalysis, fluctuates within a reasonable range, with fluctuation rate intervals of −10%–+10%, which shows that the formation rate of NO_2^- in equilibrium with the consumption rate of NO_2^- in this

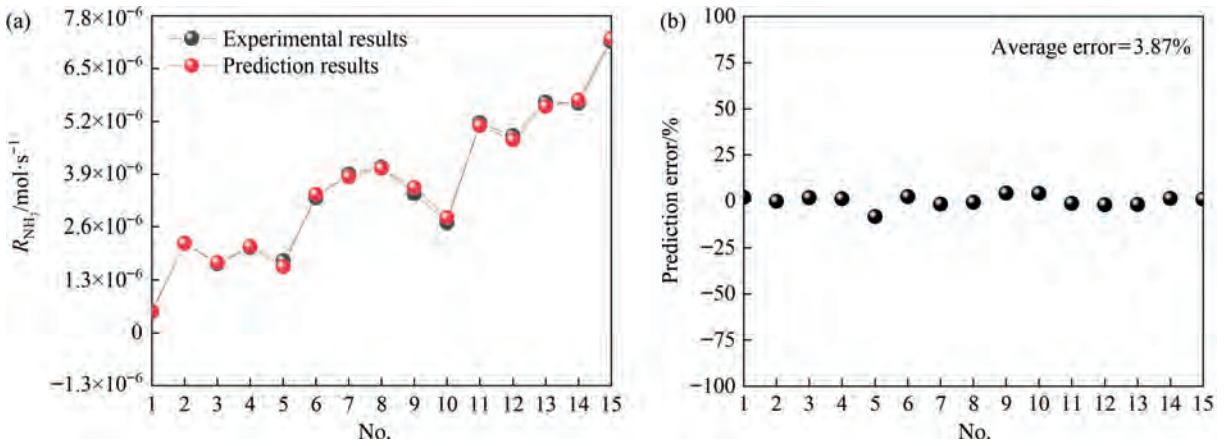

Fig. 10. (a) Data comparison between experiment and prediction, and (b) prediction error.

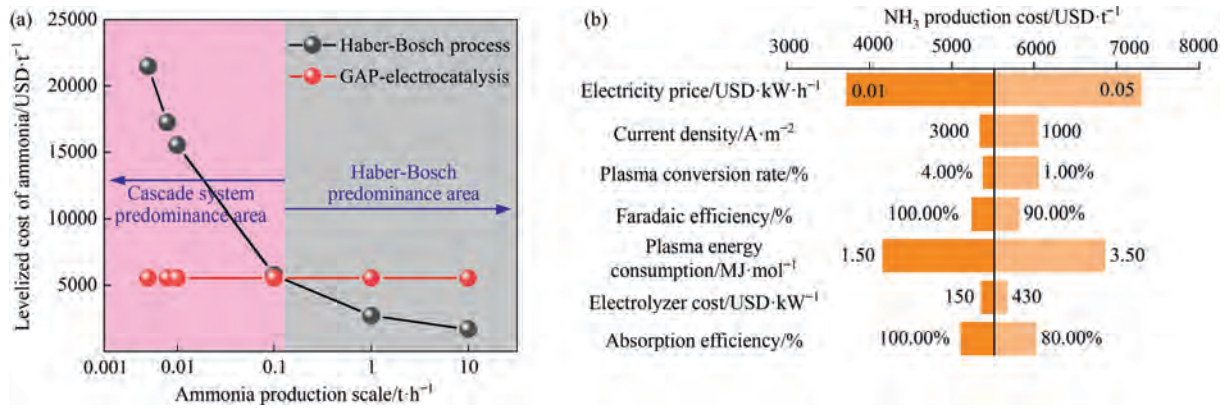

Fig. 12. (a) Economic comparison between cascade process and Haber-Bosch process; (b) Single variable sensitivity analysis for the LCOA in cascade process.

system, thus directly proving the correctness of the empirical equation constructed based on the RSA method, and providing the feasibility solution to achieve dynamic matching of NO_2^- in front and back ends of the cascade system.

3.3. Techno-economic assessment of the cascaded system

A techno-economic assessment (TEA) model was developed for the gliding arc plasma-coupled electrocatalytic ammonia synthesis system and the levelized cost of ammonia (LCOA) was calculated based on Eq. (9) [33] in order to evaluate the economic benefits of the cascade system.

$$\mathrm{LCOA} = \frac{C_{\mathrm{invest}} + \mathrm{Rep}_{\mathrm{cost}} + \frac{\sum_{i=1}^{N} C_{\mathrm{O\&M}-i}}{\sum_{i=1}^{N}(1+r)^i}}{\sum_{i=1}^{N} \frac{n_{\mathrm{NH_3}}}{(1+r)^i}} \tag{9}$$

where N is the plant lifetime; r is the discount rate, which is generally set to 7.5% for green ammonia [34]; C_{invest}, $\mathrm{Rep}_{\mathrm{cost}}$ and $C_{\mathrm{O\&M}\text{-}i}$ are the total capital investment, total replacement cost and operation-maintenance cost, respectively; and n is the annual production capacity of ammonia.

Taking a distributed small-scale green ammonia synthesis plant with an annual production capacity of 10 tons as an example, the LCOA was calculated, and the calculation process is detailed in the Supporting Information.

Based on the calculation results of C_{invest}, $\mathrm{Rep}_{\mathrm{cost}}$ and $C_{\mathrm{O\&M}\text{-}i}$, the levelized cost of ammonia from the gliding arc plasma-coupled electrocatalytic cascade system was calculated by Eq. (9). Fig. 12(a) compares the LCOA of Haber-Bosch process [21] and cascade process at different production scales. In a small-scale (<0.1 $t \cdot h^{-1}$) distributed green ammonia production mode, the cascade process is more economical than Haber-Bosch process under the baseline conditions shown in Table S2, which shows the great potential of the cascade process for small-scale green ammonia synthesis at this stage. In addition, the distributed configuration is more flexible than the centralized plant, which helps to significantly reduce the additional costs and CO_2 emissions associated with the transportation of ammonia from the production site to the consumption site.

However, the economic advantage of the cascade process gradually disappears as the production scale is expanded. In order to extend the economic feasibility of the cascade system on the larger scale, the sensitivity analysis was conducted to clarify the contribution of each variable to the LCOA, so as to explore the potential solutions to reduce the LCOA, the results are shown in Fig. 12(b).

The variation of LCOA induced by current density, plasma conversion rate, Faradaic efficiency, electrolyzer cost and absorption efficiency is nonlinear, expressed as the asymmetric structure of the plotted bar plots. Therefore, over-optimization of these parameters will result in diminishing gains in LCOA reduction. Among all the parameters involved in the single-variable sensitivity analysis, reductions in electricity price and GAP energy consumption have the greatest potential for LCOA reduction. Specifically, the LCOA will be reduced by 32.54% and 24.51% when the electricity price is reduced to 0.01 $USD \cdot kW \cdot h^{-1}$ or the plasma energy consumption is reduced to 1.5 $MJ \cdot mol^{-1}$, respectively. It should be pointed out that the effects of GAP energy consumption on LCOA are reflected in twofold: plasma equipment input and electricity consumption. When the GAP energy consumption is reduced from 2.5 $MJ \cdot mol^{-1}$ to 1.5 $MJ \cdot mol^{-1}$, the LCOA is reduced by 1350.97 $USD \cdot t^{-1}$, of which the contributions from the GAP equipment input and electricity consumption to the LCOA reduction are 57.56% and 42.44%. From the long-term perspective, with the development and improvement of various green power technologies and related supporting equipment, the reduction of power generation costs will inject the steady stream of vitality into the engineering construction of plasma-coupled electrocatalytic green ammonia synthesis technology.

4. Conclusions

In this paper, a gliding arc plasma-coupled electrocatalytic ammonia synthesis cascade system was designed and constructed, and the effects of key operating conditions on the formation rates of NO_2^- and NH_3, such as plasma generator input voltage, air flow rate, electrolyzer cell voltage and cathode electrolyte flow rate, were systematically analyzed. Further, the empirical equation between the NO_2^- consumption rate and electrocatalytic operation parameters was constructed based on the RSA methodology, and the combination of electrocatalytic operation parameters under the specific NO_2^- formation rate was obtained, which led to the stable operation of cascade system for 10 h. Finally, a TEA model was developed to account for the LCOA from the cascade system and the single-variable sensitivity analysis was performed to provide solutions for LCOA reduction. The main conclusions are as follows:

(1) The $R_{\mathrm{NH_3}}$ was highly correlated with the NO_2^- initial concentration, attributed to the fact that the higher initial concentration elevated the concentration gradient at the

catalyst-electrolyte interface, which was beneficial to enhance the concentration diffusion rate, and thus facilitated the interfacial electrocatalytic reaction;

(2) Based on the RSA method, nonlinear empirical equation between R_{NH_3} and electrolyzer cell voltage, NO_2^- initial concentration and cathode electrolyte flow rate were obtained, and the average prediction error of the equation for R_{NH_3} was only 2.30%;

(3) Based on the empirical equation, the combination of electrocatalytic operating conditions which match the $R_{NO_2^-}$ at the plasma generation input voltage of 200 V and the air flow rate of 4.0 $L \cdot min^{-1}$ was obtained, such that the fluctuation of NO_2^- concentration during the experiment is from −10% to +10%.

(4) The TEA model of the cascade system was developed to account for the LCOA. The results show that the cascade system is more economical than Haber-Bosch process at the ammonia production scales less than 0.1 $t \cdot h^{-1}$. In addition, single variable sensitivity analysis showed that lower electricity prices and plasma energy consumption are the most favorable ways to reduce the LCOA in the cascade system.

CRediT Authorship Contribution Statement

Yang Lv: Writing – original draft, Validation, Methodology, Investigation, Formal analysis, Data curation, Conceptualization. Gaoyang Li: Writing – original draft, Methodology, Formal analysis. Jianpeng Sun: Writing – original draft, Conceptualization. Honghui Ou: Writing – original draft, Supervision. Yang Li: Writing – original draft, Supervision, Resources, Project administration, Conceptualization. Guidong Yang: Writing – review & editing, Supervision, Resources, Conceptualization.

Data Availability Statement

The data that support the findings of this study are available on request from the corresponding author.

Declaration of Competing Interest

The authors declare that they have no known competing financial interests or personal relationships that could have appeared to influence the work reported in this paper.

Acknowledgements

This research was financially supported by National Key Research and Development Program of China (2020YFA0710000), National Natural Science Foundation of China (U22A20391, 22308274), Postdoctoral Fellowship Program of CPSF (GZB20240600, 2023TQ0265, 2024M752589), Innovation Capability Support Program of Shaanxi (NO. 2023-CX-TD-26), and the Programme of Introducing Talents of Discipline to Universities (B23025).

Supplementary Material

Supplementary data to this article can be found online at https://doi.org/10.1016/j.cjche.2025.04.014.

References

[1] V. Jain, S. Tyagi, P. Roy, P.P. Pillai, Ammonia synthesis with visible light and quantum dots, *J. Am. Chem. Soc.* 146 (47) (2024) 32356–32365.
[2] Q.K. Hu, O.W. Peng, J. Liu, D.R. Chen, K.P. Loh, Low power consumption ammonia electrosynthesis using hydrogen-nitrate flow electrolyzer, *ACS Energy Lett.* 9 (5) (2024) 2303–2309.
[3] X. Fu, J.B. Pedersen, Y. Zhou, M. Saccoccio, S. Li, R. Sažinas, K. Li, S.Z. Andersen, A. Xu, N.H. Deissler, J.B.V. Mygind, C. Wei, J. Kibsgaard, P.C.K. Vesborg, J.K. Nørskov, I. Chorkendorff, Continuous-flow electrosynthesis of ammonia by nitrogen reduction and hydrogen oxidation, *Science* 379 (6633) (2023) 707–712.
[4] K.E. Lamb, M.D. Dolan, D.F. Kennedy, Ammonia for hydrogen storage; A review of catalytic ammonia decomposition and hydrogen separation and purification, *Int. J. Hydrogen Energy* 44 (7) (2019) 3580–3593.
[5] S.L. Foster, S.I.P. Bakovic, R.D. Duda, S. Maheshwari, R.D. Milton, S.D. Minteer, M.J. Janik, J.N. Renner, L.F. Greenlee, Catalysts for nitrogen reduction to ammonia, *Nat. Catal.* 1 (7) (2018) 490–500.
[6] Y.C. Wan, J.C. Xu, R.T. Lv, Heterogeneous electrocatalysts design for nitrogen reduction reaction under ambient conditions, *Mater. Today* 27 (2019) 69–90.
[7] S. Padinjarekutt, H.Z. Li, S.J. Ren, P. Ramesh, F.L. Zhou, S.G. Li, G. Belfort, M. Yu, Na^+-gated nanochannel membrane for highly selective ammonia (NH_3) separation in the Haber-Bosch process, *Chem. Eng. J.* 454 (2023) 139998.
[8] J. Emsley, Going one better than nature? *Nature* 410 (6829) (2001) 633–634.
[9] S. Samaroo, D.P. Hickey, Electrochemical ammonia production from nitrates in agricultural tile drainage: technoeconomic and global warming analysis, *AIChE J.* 69 (2) (2023) e17969.
[10] K. Dong, Y.C. Yao, H.B. Li, H. Li, S.J. Sun, X. He, Y. Wang, Y.S. Luo, D.D. Zheng, Q. Liu, Q. Li, D.W. Ma, X.P. Sun, B. Tang, H_2O_2-mediated electrosynthesis of nitrate from air, *Nat. Synth* 3 (6) (2024) 763–773.
[11] A.J. Martín, T. Shinagawa, J. Pérez-Ramírez, Electrocatalytic reduction of nitrogen: from Haber-Bosch to ammonia artificial leaf, *Chem* 5 (2) (2019) 263–283.
[12] X.L. Xue, R.P. Chen, C.Z. Yan, P.Y. Zhao, Y. Hu, W.J. Zhang, S.Y. Yang, Z. Jin, Review on photocatalytic and electrocatalytic artificial nitrogen fixation for ammonia synthesis at mild conditions: advances, challenges and perspectives, *Nano Res.* 12 (6) (2019) 1229–1249.
[13] H.M. Liu, N. Guijarro, J.S. Luo, The pitfalls in electrocatalytic nitrogen reduction for ammonia synthesis, *J. Energy Chem.* 61 (2021) 149–154.
[14] M. Hattori, S. Iijima, T. Nakao, H. Hosono, M. Hara, Solid solution for catalytic ammonia synthesis from nitrogen and hydrogen gases at 50 °C, *Nat. Commun.* 11 (1) (2020) 2001.
[15] S. Feng, W.B. Gao, J.P. Guo, H.J. Cao, P. Chen, Electrodriven chemical looping ammonia synthesis mediated by lithium imide, *ACS Energy Lett.* 8 (3) (2023) 1567–1574.
[16] Y.W. Ren, C. Yu, L.S. Wang, X.Y. Tan, Z. Wang, Q.B. Wei, Y.F. Zhang, J.S. Qiu, Microscopic-level insights into the mechanism of enhanced NH_3 synthesis in plasma-enabled cascade N_2 oxidation-electroreduction system, *J. Am. Chem. Soc.* 144 (23) (2022) 10193–10200.
[17] W. Liu, M.Y. Xia, C. Zhao, B. Chong, J.H. Chen, H. Li, H.H. Ou, G.D. Yang, Efficient ammonia synthesis from the air using tandem non-thermal plasma and electrocatalysis at ambient conditions, *Nat. Commun.* 15 (1) (2024) 3524.
[18] I. Muzammil, Y.N. Kim, H. Kang, D.K. Dinh, S. Choi, C. Jung, Y.H. Song, E. Kim, J. M. Kim, D.H. Lee, Plasma catalyst-integrated system for ammonia production from H_2O and N_2 at atmospheric pressure, *ACS Energy Lett.* 6 (8) (2021) 3004–3010.
[19] X.Q. Yan, Y. Zhao, Y.Z. Zhang, B.W. Wang, H.H. Fan, H.H. Ou, X.L. Hou, Q.Z. Huang, H.G. Hu, G.D. Yang, A five-fold twin structure copper for enhanced electrocatalytic nitrogen reduction to sustainable ammonia, *AIChE J.* 71 (3) (2025) e18654.
[20] J. Yang, T.Y. Li, C.S. Zhong, X.X. Guan, C. Hu, Nitrogen fixation in water using air phase gliding arc plasma, *J. Electrochem. Soc.* 163 (10) (2016) E288–E292.
[21] A.J. Wu, J. Yang, B. Xu, X.Y. Wu, Y.H. Wang, X.J. Lv, Y.C. Ma, A.N. Xu, J.G. Zheng, Q.H. Tan, Y.Q. Peng, Z.F. Qi, H.F. Qi, J.F. Li, Y.L. Wang, J. Harding, X. Tu, A.Q. Wang, J.H. Yan, X.D. Li, Direct ammonia synthesis from the air *via* gliding arc plasma integrated with single atom electrocatalysis, *Appl. Catal. B Environ.* 299 (2021) 120667.
[22] J. Ding, W.Y. Li, Q.Q. Chen, J.F. Liu, S. Tang, Z.W. Wang, L.W. Chen, H.M. Zhang, Sustainable ammonia synthesis from air by the integration of plasma and electrocatalysis techniques, *Inorg. Chem. Front.* 10 (19) (2023) 5762–5771.
[23] Y. Lv, J.H. Chen, P.W. Bai, T. Xie, J.J. Liu, H.H. Ou, G.D. Yang, Mass transfer and electrochemical behavior of nitrate reduction to ammonia in electrocatalytic flow cell reactor, *AIChE J.* 70 (1) (2024) e18262.
[24] Y.T. Wang, C.H. Wang, M.Y. Li, Y.F. Yu, B. Zhang, Nitrate electroreduction: mechanism insight, *in situ* characterization, performance evaluation, and challenges, *Chem. Soc. Rev.* 50 (12) (2021) 6720–6733.
[25] X.Y. Dai, L. Tian, Z.X. Liu, W.S. Xu, Y.P. Liu, Y. Liu, Nanoreactor based on cyclodextrin for direct electrocatalyzed ammonia synthesis, *ACS Nano* 16 (11) (2022) 18398–18407.
[26] D. Yin, D. Chen, Y.X. Zhang, W.J. Wang, Q. Quan, W. Wang, Y. Meng, Z.X. Lai, Z. Yang, S. Yip, C.Y. Wong, X.M. Bu, X.Y. Wang, J.C. Ho, Synergistic active phases of transition metal oxide heterostructures for highly efficient ammonia electrosynthesis, *Adv. Funct. Mater.* 33 (50) (2023) 2303803.
[27] Y.F. Zhang, C. Zhu, H.X. Wei, Y. Tian, W.D. Xia, C. Wang, A highly effective N_2 fixation method based on reverse vortex flow gliding arc plasma under water, *J. Clean. Prod.* 452 (2024) 142158.
[28] Y. Lv, W.K. Teng, Y. Li, H.H. Ou, T. Xie, X.Q. Yan, G.D. Yang, Electrochemical macrokinetics analysis of nitrite electrocatalytic reduction to ammonia, *AIChE J.* 70 (12) (2024) e18578.

[29] B.S. Patil, F.J.J. Peeters, G.J. van Rooij, J.A. Medrano, F. Gallucci, J. Lang, Q. Wang, V. Hessel, Plasma assisted nitrogen oxide production from air: using pulsed powered gliding arc reactor for a containerized plant, *AIChE J.* 64 (2) (2018) 526–537.
[30] S. Yang, A. Chen, Z.J. Tang, Z.X. Wu, P. Li, Y.B. Wang, X.Q. Wang, X. Jin, S.C. Bai, C.Y. Zhi, Regulating the electrochemical reduction kinetics by the steric hindrance effect for a robust Zn metal anode, *Energy Environ. Sci.* 17 (3) (2024) 1095–1106.
[31] A.A. Shah, M.J. Watt-Smith, F.C. Walsh, A dynamic performance model for redox-flow batteries involving soluble species, *Electrochim. Acta* 53 (27) (2008) 8087–8100.
[32] O.A. El-Shafie, R.M. El-Maghraby, J. Albo, S.K. Fateen, A. Abdelghany, Modeling and numerical investigation of the performance of gas diffusion electrodes for the electrochemical reduction of carbon dioxide to methanol, *Ind. Eng. Chem. Res.* 59 (47) (2020) 20929–20942.
[33] H. Bouaboula, M. Ouikhalfan, I. Saadoune, J. Chaouki, A. Zaabout, Y. Belmabkhout, Addressing sustainable energy intermittence for green ammonia production, *Energy Rep.* 9 (2023) 4507–4517.
[34] L. Hatton, R. Bañares-Alcántara, S. Sparrow, F. Lott, N. Salmon, Assessing the impact of climate change on the cost of production of green ammonia from offshore wind, *Int. J. Hydrogen Energy* 49 (2024) 635–643.